DESIGN OF MARINE VEHICLE POWERED BY MAGNETOHYDRODYNAMIC THRUSTER

Cherng-Shyong Chan [1,2], *Jia-Hong Cheng* [2], *Cing-Hui Zeng* [3],
Jen-Rung Huang [4], *Yu-Hsuan Chen* [2], *Yen-Ju Chen* [3],
Thi Trang Pham [5], *Wei-Hsiang Chao* [6], *Jen-Tzong Jeng* [5],
Tsung-Long Liu [2,4], *Kuan-Cheng Pan* [2,4],
Yan-Hom Li [2,3], *Ching-Yao Chen* [2]

[1] *Department of Mechanical Engineering, National Yunlin University
of Science and Technology, Taiwan, R.O.C.*
[2] *Department of Mechanical Engineering, National Chiao Tung University, Taiwan, R.O.C.*
[3] *Department of Mechanical and Aerospace Engineering, Chung Cheng Institute
of Technology, National Defense University, Taiwan R.O.C.*
[4] *Department of Power Vehicle and Systems Engineering, Chung Cheng Institute
of Technology, National Defense University, Taiwan, R.O.C.*
[5] *Department of Mechanical Engineering, National Kaohsiung University
of Science and Technology, Taiwan, R.O.C.*
[6] *Materials and Electro-Optics Research Division, National Chung-Shan Institute
of Science and Technology, Taiwan R.O.C.*
e-Mail: pankc@url.com.tw, yanhom@ndu.edu.tw, chingyao@mail.nctu.edu.tw

The present study outlines the design of a magnetohydrodynamic (MHD) thruster system which is capable to power a 3-meter ship model cruising at a speed of $V = 0.5\,\text{m/s}$ using the Lorentz force generated by the electric field and magnetic field in conducting seawater. Based on the computational fluid dynamics (CFD) simulation of a modified Delft 372 catamaran model, the thrust needed to achieve the targeted cruising speed is first estimated. To achieve the estimated magnitude of the thrust, dimensions of thruster modules are designed based on numerical simulations of magnetic field, for better distributions of the strength and uniformity of the magnetic field. Additional CFD simulations of the flows through the thruster module, coupled with magnetic and electric fields, are conducted to realize the hydrodynamics. Consequently, several configurations of thruster modules are manufactured and experimented. A particular configuration of a shielded two-unit module is chosen to power the ship model. Finally, a complete system of MHD-1 marine vehicle, including a ship model, multiple MHD thruster modules and power suppliers, is assembled and tested. The system is shown capable to cruise closely to the targeted speed.

Introduction. Magnetohydrodynamics (MHD) is a unique branch of fluid dynamics concerned with the dynamics and behavior of conducting fluids affected by magnetic and electric fields. The typical conducting magnetofluids include plasma, liquid metals, salt water and electrolytes. By using the Lorentz force generated by the perpendicularly imposed magnetic field and electric current, the applications of MHD have been of interest to engineers since its initiation in the 1940's [1], e.g., propulsion systems [2–12], pumps [13, 15–17], motor [18], heat transfer devices [19], metal processes [20] and generators [21]. Among them, MHD propulsion applied to marine vehicles has been a long and active field, since first proposed in [2] in the 1960's because of the conductive property of seawater to achieve a propellerless power system. In the following developments, superconductors were applied to generate MHD propulsion [3, 4] as an extremely strong magnetic field is required to achieve a better electrical efficiency, e.g., about 40% efficiency at 5 Tesla [6]. However, the heavy weight as well as the complexity of the su-

perconductor prevented the practical uses of MHD propulsion. Nevertheless, the study of MHD propulsion was continued for several decades. In 1988, the capability of MHD propulsion in a ship was successfully demonstrated [5], and large-scale vehicles were able to be powered by MHD thrusters, for instance, the MHD-propelled Yamato 1 [9] and HEMS-1 [10] built in the 1990's. It has been widely reported that the progresses in developing MHD-propelled submarines are ongoing in recent years, e.g., news reported in [22]. Taking the advantages of the advancement of key technologies of magnetism and design tools, such as permanent magnets of neodymium iron boron, lithium batteries and powerful numerical software, we intend to develop a small scale marine unmanned surface vehicle (USV) using permanent magnets. In addition, the designed marine MHD USV possesses the potential ability of thrust vector control (TVC) by installing multiple thruster units. The MHD USV is expected to perform special tasks, of which stealth and maneuverability are crucial, even the electric efficiency might be extremely low. The details of the design procedures and tested results are reported in the present paper.

At the first stage of design, the major concern of the marine MHD USV is mainly the net propulsion, which involves the MHD thrust and hydrodynamic drag, so that understanding of the magnetic, electric and flow fields is crucial. The governing equations of hydrodynamics with the incorporated Lorentz force in an incompressible Newtonian fluid are expressed as the augmented Navier–Stokes equations [18]

$$\nabla \cdot \mathbf{u} = 0, \tag{1}$$

$$\rho \left[\frac{\partial \mathbf{u}}{\partial t} + (\mathbf{u} \cdot \nabla)\mathbf{u} \right] = -\nabla p + \mu \nabla^2 \mathbf{u} + \mathbf{F}_{\mathrm{L}}. \tag{2}$$

Here, t, $\mathbf{u}$, p, μ and ρ denote, respectively, the time, velocity vector, pressure, viscosity and density of the conducting fluid. $\mathbf{F}_{\mathrm{L}}$ represents the force density of the Lorentz force and takes the form of

$$\mathbf{F}_{\mathrm{L}} = (\mathbf{J} \times \mathbf{B}), \tag{3}$$

where $\mathbf{J}$ and $\mathbf{B}$ are the current density and the magnetic field, respectively and are derived by the Maxwell equation and Ohm's law given as

$$\nabla \cdot \mathbf{B} = 0, \tag{4}$$

$$\mathbf{J} = \sigma[-\nabla\psi + (\mathbf{u} \times \mathbf{B})]. \tag{5}$$

Here σ and ψ are the electric conductivity and the electric potential, respectively. For a sufficiently conducting medium, the electric charge is conserved, i.e. $\nabla \cdot \mathbf{J} = 0$, so that the electric potential equation is governed by

$$\nabla^2 \psi = \nabla \cdot (\mathbf{u} \times \mathbf{B}). \tag{6}$$

These equations will be solved numerically to provide guidelines for better design.

1. Results and discussion.

1.1. Design of the ship model. The present study aims to power a scaled-down ship model by the MHD thrusters with a cruising speed of $V = 0.5\,\mathrm{m/s}$. The dimensions of the ship model, named MHD-1 modified from the Delft 372 catamaran model [23], is shown in Fig. 1. It has been well concluded that the resistance on the surface ship is induced both by the viscous skin friction and by the gravitational surface waves. To estimate the needed thrust, i.e. the total induced drag of the sailing ship model, a numerical
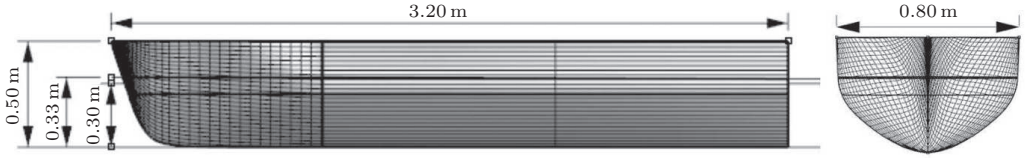
Fig. 1. Geometry and dimension of the modified Delft 372 catamaran model designed in the present study.
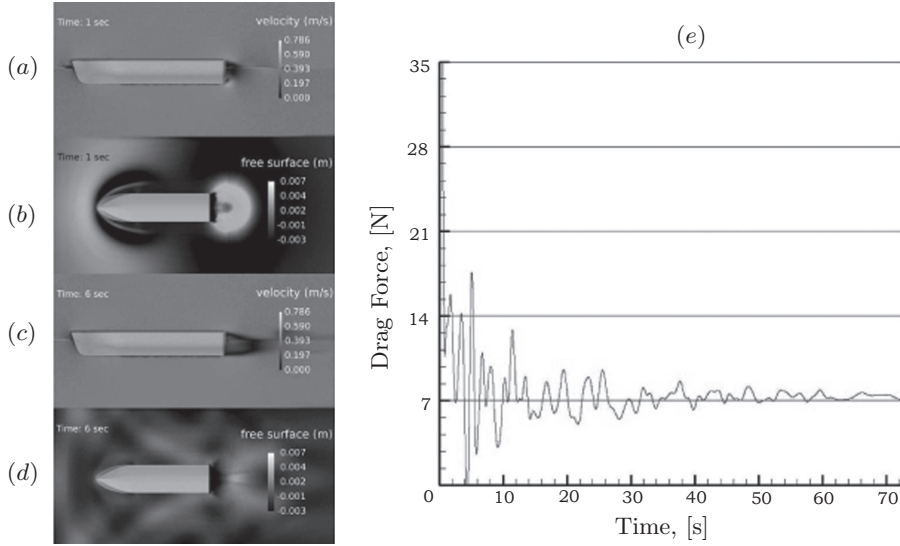

Fig. 2. Flow field $(a),(c)$ and wave height $(b),(d)$ at $t = 1$ and 6 s; (e) temporal evolution of the total drag obtained by numerical simulation of the ship model with a cruising speed of $V = 0.5$ m/s.

simulation was carried out to solve the full 3D unsteady Reynolds–Averaged–Navier–Stokes (RANS) equations. The computational domain (30 m $\times$ 6 m $\times$ 2.5 m) includes the seawater (or the air) beneath (or above) the surface. The viscosity and density of the seawater and air are taken as $\mu_{\text{water}} = 9.7 \times 10^{-4}$ kg/m·s, $\rho_{\text{water}} = 1.023 \times 10^3$ kg/m^3 and $\mu_{\text{air}} = 1.789 \times 10^{-5}$ kg/m ·s, $\rho_{\text{air}} = 1.225$ kg/m^3, respectively. The turbulent effects are dealt with the k-ϵ model. The ship model is designed to have a draught of 0.33 m beneath the seawater surface with a displacement of 525 kg and encounter a free stream velocity of $V = 0.5$ m/s. The Volume of Fluid (VOF) method is applied to capture the waving surface of seawater. The set of equations is numerically solved by ANSYS Fluent [24], and the results are shown in Fig. 2.

Figs. 2a,c and b,d show the velocity distribution in the middle cross-section from the side and the wave height on the surface from top, respectively, at $t = 1$ s and 6 s. When the ship model just starts to move from rest at $t = 1$ s, strong induced wakes associated with the significant heights of the wave at the bow and stern of the ship are clearly observed. The presence of the strong wake and high wave results in significant resistance, as shown at very early time in Fig. 2e. As time proceeds, the wake and the wave on the surface continuously get weaker, e.g., $t = 6$ s shown in Figs. 2c,d. This strong
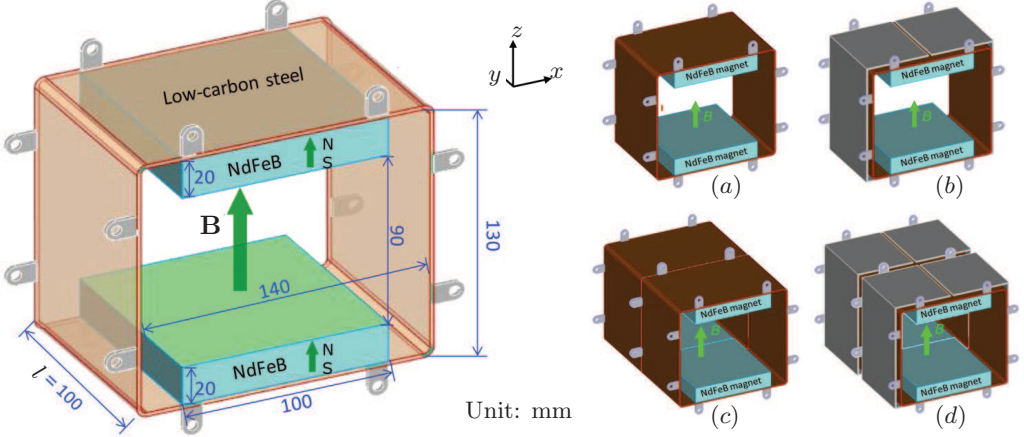
Fig. 3. (Left) Geometry and dimension of a single MHD thruster unit. Four configurations of thruster modules are considered: (*a*) single-unit module, (*b*) shielded single-unit module, (*c*) two-unit module, and (*d*) shielded two-unit module.

transit phenomenon leads to a significant fluctuation of the total resistance till $t \approx 40\,\text{s}$, as also shown in Fig. 2*e*, and eventually evolves to a nearly constant value about $7\,\text{N}$ after $t > 40$. This nearly steady resistance of $7\,\text{N}$ serves as a reference value to design the MHD thrusters, whose total thrust should be capable to overcome the resistance and to power the ship model for steady cruise.

1.2. Design of MHD thruster module. The thrust by the Lorentz force (T_L) depends on the external magnetic field, so that the strength and distribution of the magnetic field are important for a better design of the thruster module. After considering the weight of the iron shell and available magnets, the dimension of a single thruster unit is proposed and shown in Fig. 3. A pair of permanent magnets of neodymium iron boron (NdFeB, N40) are placed at the bottom and top of the soft-iron shell. Note that different thicknesses of the shell have been tested, and the thicker shell always results in higher magnetic strength inside the thruster, as expected. Nevertheless, considering the weight constraint, a 2-mm iron shell was chosen to optimize the field-to-weight ratio of the MHD thruster. Four configurations of the thruster modules were considered, as also shown in Fig. 3, such as (*a*) a single-unit module, (*b*) a single-unit module with additional shielding by a NiFe alloy, (*c*) a two-unit module, and (*d*) a two-unit module with additional shielding. Detailed distributions of magnetic fields for these four configurations are simulated by ANASYS Maxwell, and the results are illustrated in Figs. 4, 5 and 6.

Fig. 4*a* shows the magnetic lines and strength distribution of the plain single-unit module by a 2D simulation. The non-uniformity of the magnetic field can be clearly observed, in which a weaker strength locates at the central region ($z = 0$), in particular, at the edges ($|x| > 25\,\text{mm}$). The full 3D simulation shown in Figs. 4*b,c* also confirms the observation. The field distribution in the cross-section at the central region, e.g., $y = 0\,\text{mm}$, as shown in Fig. 4*b*, is between $B = 0.1 \sim 0.27\,\text{T}$, with an average of $B_\text{avg} = 0.194\,\text{T}$. The field strength and uniformity deteriorate at the outer position of the thruster module ($|y| > 0$). Shown in Fig. 4*c*, the field strength is at the cross-section of $y = \pm 25\,\text{mm}$, where are the positions of 1/4 and 3/4 length of the thruster unit (total $100\,\text{mm}$, as shown in Fig. 3). The variation of the field strength is enhanced with a weaker average
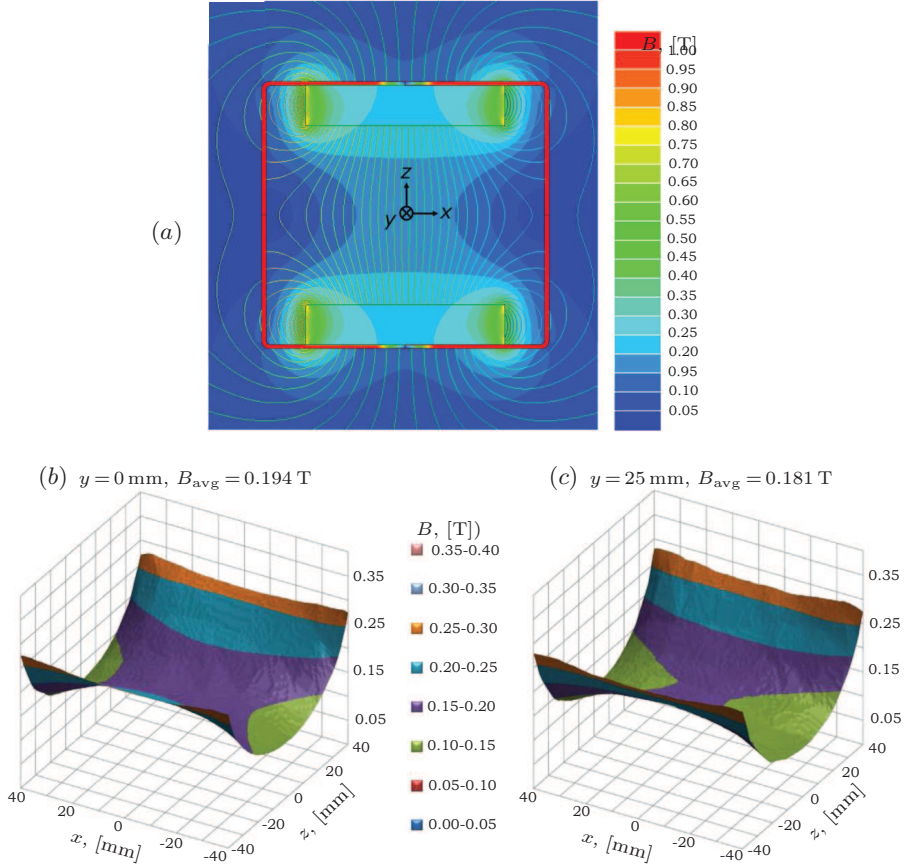
Fig. 4. (a) Magnetic lines and strength distribution of a plain single-unit module obtained by 2D simulation. The flux lines are not shown in the iron shell, where magnetization saturation occurs. The strength distribution was obtained by 3D simulation at the cross-section at (b) $y = 0$ mm and (c) $y = \pm 25$ mm.

of $B_{\mathrm{avg}} = 0.181$ T. Also observed in Fig. 4a is the significant leakage of the magnetic flux outside the shell because of the magnetization saturation in the iron shells. These results lead to two major drawbacks: (1) the dramatic decrease of the magnetic strength away from the magnets, and (2) the significant leakage of the magnetic flux.

Based on the results shown in Fig. 4, a shielded two-unit module is considered, i.e. the configuration shown in Fig. 3d. By connecting the two units in series, the region with a dramatic drop of the strength at the edges may be minimized. In addition, the magnetic leakage could also be improved with outer NiFe alloy shielding. The simulation results of the shielded two-unit module are displayed in Fig. 5. The average field strengths in the cross-sections at the center ($y = 0$ mm) and at $1/4$ (or $3/4$) length ($y = \pm 50$ mm) are increased to $B_{\mathrm{avg}} = 0.21$ T and 0.205 T, respectively, which are improved significantly.

The sample modules of these four configurations were manufactured, and their corresponding field strengths along the central axis ($x = 0$ and $z = 0$) were measured by a Gauss meter, as shown in Fig. 6. In general, the measured strengths are in good agreement with the simulations. As suggested by the simulations, the strength is stronger with
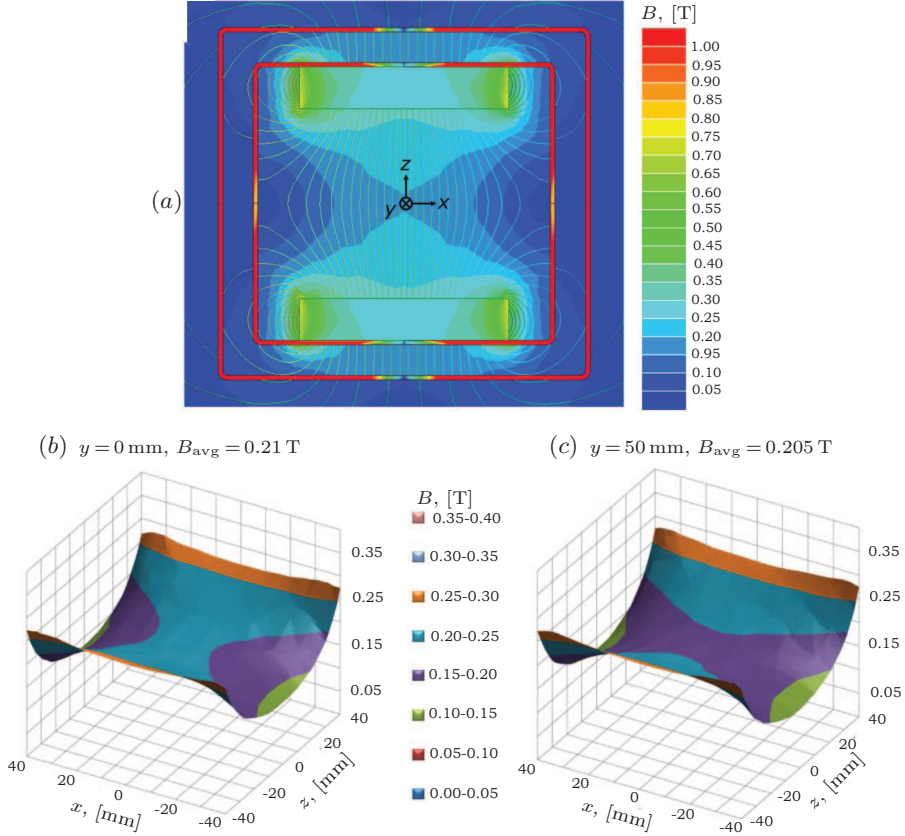
Fig. 5. (*a*) Magnetic lines and strength distribution of a shielded two-unit module obtained by 2D simulation. The flux lines are not shown in the iron shell, where magnetization saturation occurs. The strength distribution was obtained by 3D simulation at the cross-section at (*b*) $y = 0$ mm and (*c*) $y = \pm 50$ mm.

shielding. In addition, the two-unit modules can elongate the region of nearly uniform strength, so that the weaker edging effect decreases. As a result, the shielded two-unit module is expected to better power the ship model.

Simulations of the current density J were also carried out to verify the better performance of the two-unit module. The design of the thruster unit is shown in Fig. 7a. To ensure a good electrical insulation, the surfaces of the NdFeB magnets and iron shell were all coated with varnish. The electrodes, which are arranged at the lateral sides of the seawater channel, were also electrically insulated with varnish at the input and output ends. The spaces between the electrodes and the lateral sides of the iron shell were filled with polyvinyl chloride (PVC) foam to further improve the electrical insulation. The electrodes are made from flat aluminum sheets with the input-and-output current leads extended outside the seawater channel. We have found that at the current as high as 120 A, only a negligible amount of the aluminum anode is dissolved at the electrolysis of salt water within an hour.

The difference in electric potential applied to these two electrodes is $\psi_E = 64$ V in the simulations concerned with the electrolytic conductivity of seawater $\sigma = 5$ S/m. For
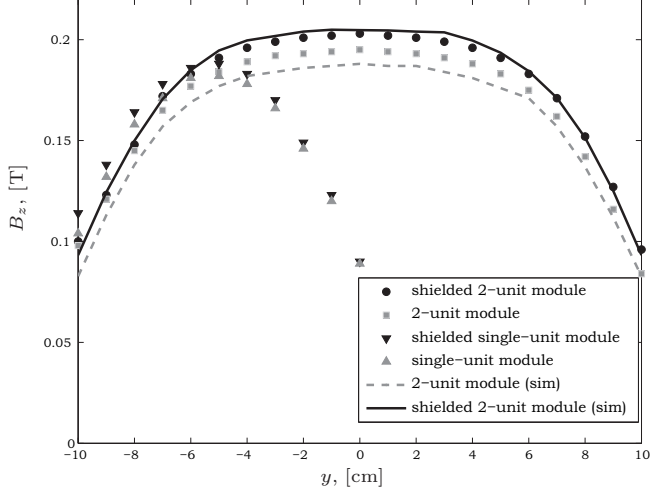
Fig. 6. Measured field strength along the *y*-axis at the central cross-section ($x = 0$ and $z = 0$). Simulated results are also shown by solid lines.
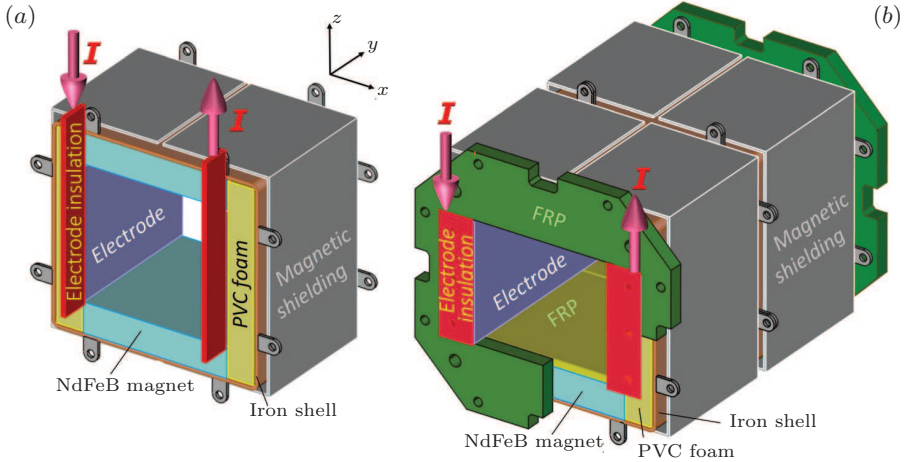

Fig. 7. Designs of (*a*) a single-unit MHD thruster with a pair of aluminum electrodes installed perpendicularly to the magnets, and (*b*) a completed two-unit thruster module. The aluminum plates fully cover the inner sides of the iron shell. The arrows show the input/output of the electric current *I*.

an ideal situation, the magnitude of the electric potential would be half the difference of the applied potential in the central section, i.e. $\psi = 32\,\text{V}$ at $x = 0$. Nevertheless, the magnitudes of the electric potential across the central section for the single-unit and two-unit modules, respectively shown in Figs. 8*a,b*, are generally less than $32\,\text{V}$. The electric potential at the middle region of the two-unit module is closer to the ideal magnitude, whereas the electric potential of the whole single-unit module is significantly smaller. The corresponding distributions of the current density are illustrated in Figs. 8*c,d*, respectively. Note that only the region inside the thruster is shown. Consistent with the
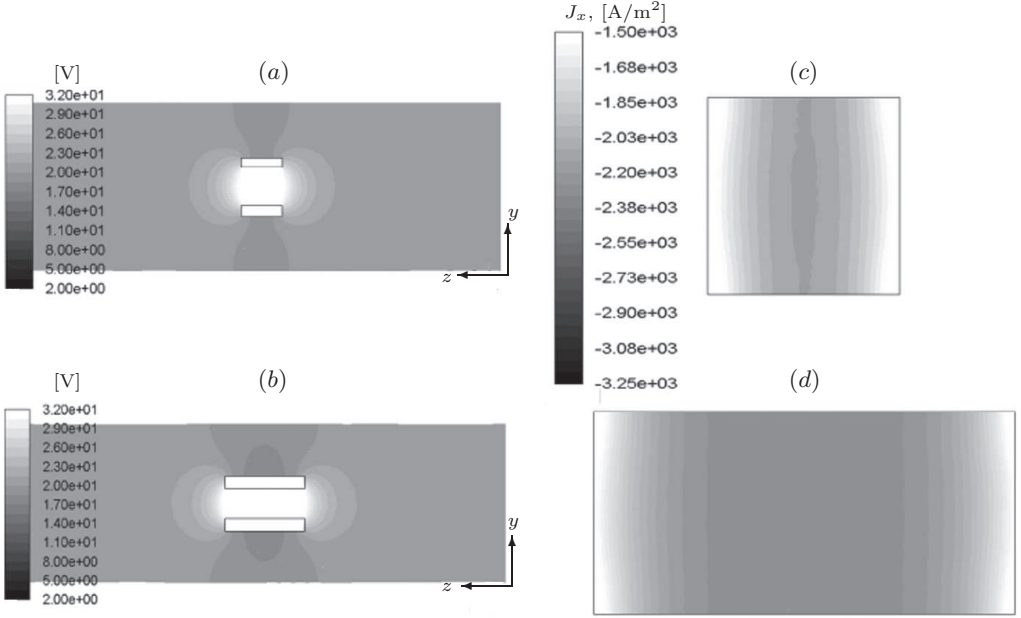
57

Fig. 8. Simulations of MHD thruster modules at the central cross-section ($x=0$) for $\psi_{\mathrm{E}} = 64\,\mathrm{V}$: ($a$) electric potential for the single-unit module; (b) electric potential for the two-unit module; (c) current density inside the single-unit module; (d) current density inside the two-unit module. The two rectangular blocks in (a) and (b) are the side views of permanent magnets. Note, (c) and (d) share the same colorscale.

distributions of the electric potential, the current density is apparently much stronger in the middle of the two-unit module. Since the Lorentz force is directly proportional to the current density, these results contribute to the better design of the two-unit module.

Based on the results obtained in the simulations of magnetic field and electric current density, the two-unit module has been chosen as the complete design shown in Fig. 7b. To overcome the strong repulsive force between the magnet modules, the NdFeB magnets were fastened to the iron shell by fiber-reinforced plastic (FRP) plates and bolts. Then, the two units were bolted together to form a two-unit module, of which the front and back ends of the thruster were covered with the FRP plates to fix the position of the magnets. The input/output current leads were bent to the end surfaces of the thruster.

1.3. Flow simulation of MHD thruster module. Numerical simulations of the flow field incorporated using the Lorentz force through the thruster module were also carried out by ANSYS Fluent to determine the performance of the thruster module of different configurations. Geometries and dimensions similar to the thruster module shown in Fig. 3 and Fig. 7 were used. Furthermore, based on the measured field strength obtained in Fig. 6, a uniformed field strength of $B_z = 0.2\,\mathrm{T}$ was assumed. By simplification, not only the Ohm's law was coupled with the Navier–Stokes equations but the Maxwell equation, too. The potential difference applied to the electrodes was $\psi_{\mathrm{E}} = 64\,\mathrm{V}$, and it yielded the average current strength $I \approx 25.9\,\mathrm{A}$ and $57.7\,\mathrm{A}$ within the thruster chamber for the single-unit and the two-unit module, respectively. Fig. 9a shows the flow induced by the Lorentz force to a stationary single-unit thruster, i.e. with no cruising speed $V = 0$.
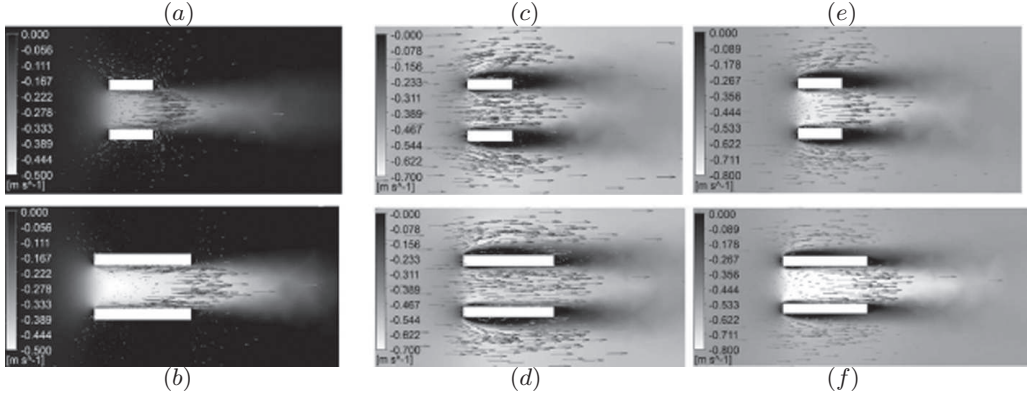
Fig. 9. Flow simulations of MHD thruster modules at the central cross-section ($x = 0$): (*a*) single-unit with $V = 0$ m/s and $B_z = 0.2$ T and $\psi_E = 64$ V; (*b*) two-unit module with $V = 0$ m/s, $B_z = 0.2$ T and $\psi_E = 64$ V; (*c*) single-unit module with $V = 0.5$ m/s, $B_z = 0$ T; (*d*) two-unit module with $V = 0.5$ m/s and $B_z = 0$ T; (*e*) single-unit module with $V = 0.5$ m/s, $B_z = 0.2$ T and $\psi_E = 64$ V; (*f*) two-unit module with $V = 0.5$ m/s, $B_z = 0.2$ T and $\psi_E = 64$ V. The two rectangular blocks are the side views of the permanent magnets.

Driven by the Lorentz force, the apparent flow is generated inside the thruster chamber, where the maximum flow speed is about 3.5 m/s. Note that the negative sign shown in the colorbar of the figure indicates the fluid flow from left to right. A mass flow rate of $Q = 2.4$ kg/s is pumped to pass through the thruster in the present condition. The induced flow is significantly enhanced for the two-unit module, as shown in Fig. 9*b*, where the maximum speed is increased to about 5 m/s. As a result, the mass flux is further raised to $Q = 3.4$ kg/s for the two-unit module. These results indicate that the present design is capable to pump a significant amount of seawater through the chamber of the thruster.

The flow field associated with the thruster module cruising at $V = 0.5$ m/s without or with the presence of the magnetic field, i.e. $B_z = 0/0.2$ T, is illustrated in Figs. 9*c*–*f*. While the mass flow rates of the single-unit and two-unit modules remain nearly unchanged at $Q = 4.6$ kg/s for $B_z = 0$, the mass flow rate is increased significantly from $Q = 5.1$ kg/s for the single-unit to $Q = 6.0$ kg/s for the two-unit module in the presence of the magnetic field $B_z = 0.2$ T. Note the increments of the mass flow rate compared with the corresponding module without the magnetic field, i.e. $\Delta Q = Q(B_z = 0.2 \text{ T}) - Q(B_z = 0 \text{ T})$ are $\Delta Q = 0.5$ and 1.4 kg/s for the single-unit and for the two-unit module, respectively. The more significant increment ΔQ for the two-unit module confirms its better performance.

1.4. Experiments with MHD thruster module. After a detailed theoretical analysis and experimental measurements, the MHD thruster modules were assembled and tested. The design of the shielded two-unit module was followed as a sample unit of the MHD thruster in Fig. 10*a*. First, to verify the better performance of the two-unit module compared to the single-unit configuration suggested by the theoretical result, experiments in a water tank were conducted. For a fair assessment, the two-unit module was directly compared with two single-unit modules. These modules are powered by a Lithium-Polymer (LiPo) battery. The actual applied current was measured at $I = 49.6$ A. The thruster modules, fully submerged in the seawater, were hung on a sliding tract with
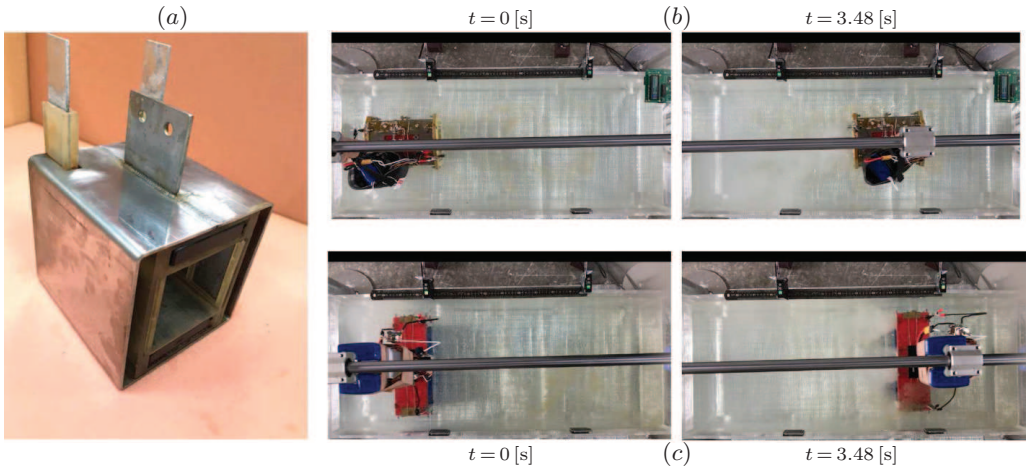
Fig. 10. (a) A sample manufactured MHD thruster unit. Experimental tests of the MHD thruster hanged on a sliding track: (b) a two-unit module, and (c) two single-unit modules.
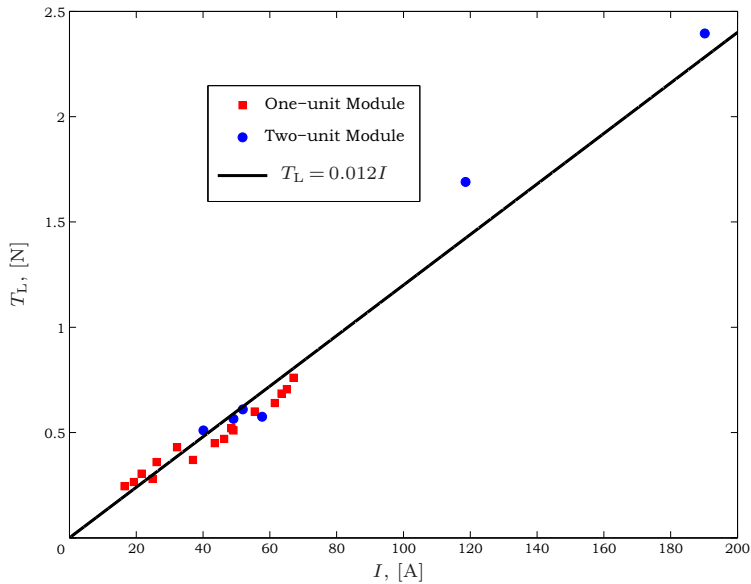

Fig. 11. Thrust (T_{L}) vs. current (I).

a negligible friction. The Lorentz force drives the thruster module moving forward once the electric current is applied. Two sensors were installed at sides of the tank to sample the average speed of the modules. Figs. 10b,c illustrate the tests of the two configurations. The photos were taken at the times when the modules reached the first sensor ($t = 0$ s) near the left side of the tank, and when the modules reached the second sensor at the right side. For both cases, apparent jet flows were generated to drive the module to move toward the right direction. The slightly faster arrival of the two-unit module supports

the better performance suggested by the theoretical analysis. Nevertheless, the speed was just about $V \approx 0.1\,\text{m/s}$, which is much less than the expected cruising speed. This is mainly because of the limitation of the testing length, so that there was no sufficient time allowed for the module to fully accelerate. The other factor is the much lower current provided. In the ship model tests, the planned current will be as high as to $I = 120\,\text{A}$.

Because of the insufficient time allowed for the tests, the MHD thrust, excluding the induced drag of a moving thruster module, was measured by a pull dynamometer. Experiments under different electric current strengths were performed, and the results are shown in Fig. 11. We would like to point out that the condition with the extremely high current $I = 190.2\,\text{A}$ was achieved by adding salt to increase the conductivity. A nearly linear correlation is followed, such that

$$T_{\text{L}} \approx 0.012 I. \tag{7}$$

The nearly linear T_{L}-I relation is consistent with the theoretical expression of the Lorentz force for a fix area. For the particular case of $I = 118.6\,\text{A}$ and $T_{\text{L}} = 1.69\,\text{N}$, which is close to the planned operating condition for the cruising speed $V = 0.5\,\text{m/s}$, the applied electric potential in salty water with 35.7 ppt of salinity was measured at $\psi_{\text{E}} = 46.4\,\text{V}$. The electric efficiency η_{E} of the MHD thruster module was obtained by

$$\eta_{\text{E}} = T_{\text{L}} V / I \psi_{\text{E}} \approx 0.000154.$$

The extremelysmall efficiency is consistent with the prediction in [6].

1.5. Test of ship model. Based on the designs presented above, an MHD-1 ship model was manufactured and multiple MHD thrusters were installed, as shown in Fig. 12. To successfully power the MHD-1 ship model with the cruising speed $V = 0.5\,\text{m/s}$, whose
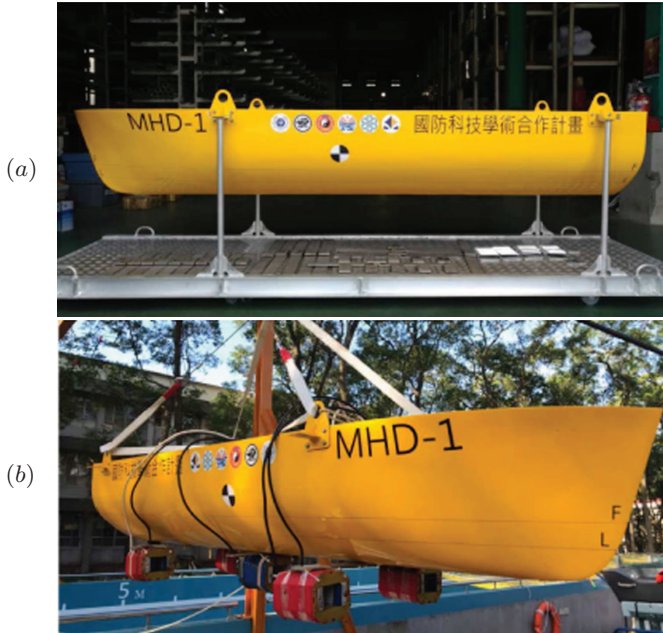

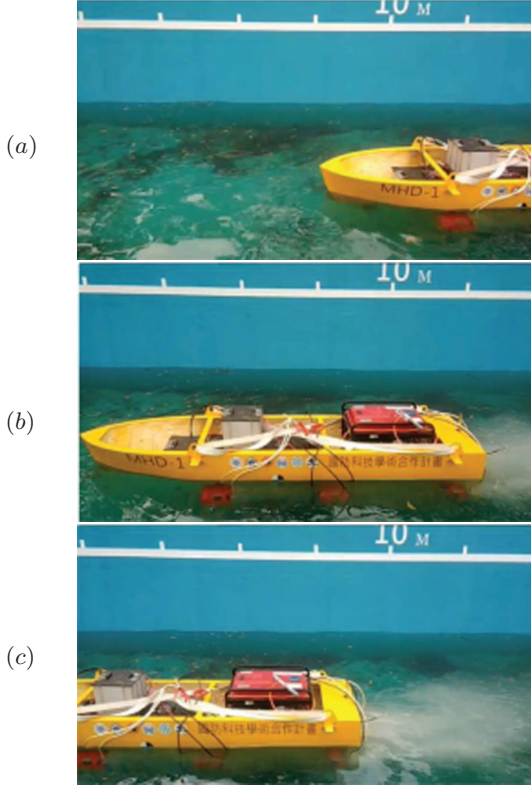*Fig. 12.* (*a*) The modified Delft 372 catamaran model MHD-1, and (*b*) with 5 MHD thruster modules installed beneath.

Fig. 13. The cruising MHD-1 ship model powered by MHDthrusters at $t = t_0$ (*a*), $t \approx t_0 + 6\,\text{s}$ (*b*) and $t \approx t_0 + 9\,\text{s}$ (*c*).

drag is about $7\,\text{N}$ according to the CFD estimation, at least five shielded two-unit modules were required provided the operating electric current $I \approx 120\,\text{A}$, based on the previous testing results. To verify the capability of the MHD thrusters, we employed 4 to 6 two-unit modules under different operating conditions with different strengths of the electric current, depending on the capacity of the power sources. Generally, the range of the cruising speed was measured at between $V = 0.25 \sim 0.5\,\text{m/s}$. A representative test is illustrated in Fig. 13, where six MHD modules (red objects beneath the ship model) are working at $I \approx 110\,\text{A}$. The four modules in the front and middle are powered by batteries, whereas the electricity for the rear two is supplied by a diesel generator. The total water displacement is about $450\,\text{kg}$. Strong jet flows are observed in Fig. 13 to provide the propulsive thrust. The cruising speed is closed to the targeted $V \approx 0.5\,\text{m/s}$, which contributes to the capability of the present design. Further improvements are in progress, including the weight reduction and streamlined thrusters. The weight reduction will be achieved by replacing the heavy generator by more efficient batteries. 3D-printed cowlings will also be attached to the front sides of the thruster modules to decrease the induced drag.

2. Concluding remarks. The present study applies MHD propulsion to design a propellerless marine vehicle driven by the Lorentz force generated by the coupling effect of the magnetic and electric fields in conducting seawater. The flow field of a cruising Delft

372 catamaran model is first simulated to obtain the necessary thrust. To acquire the better configuration of the MHD thruster module, numerical simulations of the magnetic field and current density were also carried out for stronger force and more uniform distribution. In addition, simulations of the flow passing through the thruster chamber were also performed to support the appropriateness of the designated configuration of MHD thrust modules. Based on the theoretical analysis and experimental measurements, the designated thruster modules were manufactured and tested. The sample MHD thruster module was verified to effectively move forward due to the Lorentz force. The gross thrust (T_L) generated by the present design of the MHD thruster module is nearly proportional to the electric current (I), such that $T_\mathrm{L} \approx 0.012I$. The results suggest the ship model can be effectively propel to motion by installing a sufficient number of thruster modules. At last, the MHD-1 ship model installed with multiple MHD thruster modules has been manufactured and tested. The testing results confirm that the goal can be closely achieved by the present design.

To conclude the study, we would like to point out that the presented manuscript merely shows the feasibility of the MHD vehicle by applying currently available permanent magnets and batteries. Much more optimization can be made for better propulsive efficiency, such as a better magnet arrangement to enhance the thrust. In addition, the hydrodynamic drag can be decreased by the lighter weight, streamlined thruster module or by the integration of the thruster module with the ship, etc. These works are in progresses to improve the performance of the MHD propulsion.

References

[1] H. ALFVEN. Existence of electromagnetic-hydrodynamic waves. *Nature*, vol. 150 (1942), pp. 405–406.

[2] W. RICE. Propulsion system. *U.S. Patent*, vol. 2997 (1961), no. 2,997,013.

[3] J. FRIAUF. Electromagnetic ship propulsion. *Journal of the American Society for Naval Engineers*, vol. 73 (1961), pp. 139–142.

[4] O. PHILLIPS. Electromagnetic ship propulsion. *Journal of Ship Research*, vol. 43 (1962), pp. 43–51.

[5] D. MITCHELL, D. GUBSER. Magnetohydrodynamic ship propulsion with superconducting magnets. *Journal of Superconductivity*, vol. 14 (1988), pp. 349–364.

[6] E.D. DOSS, H.K. GEYER . The need for superconducting magnets for MHD seawater propulsion. *In: Proc. the 25th Intersociety Energy Conversion Engineering Conference*, 1990.

[7] J. THIBAULT, A. ALEMANY, A. PILAUD. Some aspects of seawater MHD thrusters. *In: Proc. MHDS91*, 1991, pp. 211–218.

[8] D. Swallom, I. Sadovnik, J. Gibbs, D. Choid. Magnetohydrodynamic submarine propulsion system performance analysis results. *In: Proc. MHDS91*, 1991, pp. 277–289.

[9] Y. Sasakawa, S. Takezawa, Y. Sugawara, Y. Kyotani. The superconducting MHD-propelled ship YAMATO-1. In: *Proc. the 4th International Conference and Exhibition: World Congress on Superconductivity*, vol. 1 (1995), pp. 167–176.

[10] L.G. Yan, Z.K. Wang, C.L. Xue, Z.Y. Gao, B.Z. Zhao. Development of the superconducting magnet system for HEMS-1 MHD model ship. *IEEE Transactions on Applied Superconductivity*, vol. 10 (2000), pp. 955–958.

[11] D. Cebron, S. Viroulet, J. Vidal, J.-P. Masson, P. Viroulet. Experimental and theoretical study of magnetohydrodynamic ship models. *PLoS ONE* , (2016), no. 12 (6), e0178599.

[12] T. Weier, V. Shatrov, G. Gerbeth . Flow control and propulsion in poor conductors. In: *Magnetohydrodynamics: Historical Evolution and Trends* (S. Molokov, R. Moreau, H.K. Moffatt (Eds.), Springer, Dordrecht, 2007), pp. 295–312.

[13] J. Jang, S. Lee. Theoretical and experimental study of MHD (magnetohydrodynamic) micropump. *Sensors and Actuators A: Physical*, vol. 80 (2000), pp. 84–89.

[14] O.M. Al-Habahbeh, M. Al-Saqq, M. Safi, T. Abo Khater. Review of magnetohydrodynamic pump applications . *Alexandria Engineering Journal*, (2016), no. 55, pp. 1347–1358.

[15] V. Dolgikh, A. Pavlinov. Experimental investigation of an MHD pump model with inclined partitions. *Magnetohydrodynamics*, vol. 53 (2017), no. 3, pp. 511–514, DOI: http://doi.org/10.22364/mhd.53.3.7

[16] V. Dolgikh, A. Pavlinov. Design optimization of the MHD pump with inclined partitions. *Magnetohydrodynamics*, vol. 55 (2019), no.1/2, pp. 39–46, DOI: http://doi.org/10.22364/mhd.55.1-2.5

[17] V.N. Timofeev, M.Yu. Khatsayuk, I.V. Kizhaev. Mathematical simulation of electromagnetic and hydrodynamic processes in the MHD pump. *Magnetohydrodynamics*, vol. 55 (2019), no. 3, pp. 337–346, DOI: http://doi.org/10.22364/mhd.55.3.6

[18] M. Haghparast, M. Pahlavani, D. Azizi. Numerical investigation of the effects of magnetic field and fluid electrical conductivity on the performance of marine magnetohydrodynamic motors. *IET Electric Power Applications*, vol. 12 (2018), no. 8, pp. 1207–1214.

[19] I.A. Belyaev, L.G. Genin, Y.I. Listratov, I.A. Melnikov, N.G. Razuvanov, V.G. Sviridov, E.V. Sviridov. Features of MHD heat transfer in simple channels. *Magnetohydrodynamics*, vol. 54 (2018), no. 3, pp. 245–260, DOI: http://doi.org/10.22364/mhd.54.3.5

[20] V. Timofeev, M. Khatsayuk, S. Timofeev. Analysis of the transverse end effect in the MHD stirrer for molten metals. *Magnetohydrodynamics*, vol. 53 (2017), no. 3, pp. 521–536, DOI: http://doi.org/10.22364/mhd.53.3.9

[21] S. CARCANGIU, R. FORCINETTI, A. MONTISCI. Simulink model of an inductive MHD generator. *Magnetohydrodynamics*, vol. 53 (2017), no. 2, pp. 255–266, DOI: http://doi.org/10.22364/mhd.53.2.4

[22] A. HOLLINGS. China Successfully Tests Near-Silent Submarine Propulsion Technology. *https://sofrep.com/news/china-successfully-tests-near-silent-submarine-propulsion-technology/,* Nov. 1, 2017.

[23] R. BROGLIA, B. JACOB, S. ZAGHI, F. STERN, A. OLIVIERI. Experimental investigation of interference effects for high-speed catamarans. *Ocean Engineering*, vol. 76 (2014), pp. 75–85.

[24] ANSYS, INC. ANSYS Fluent Theory Guide (ANSYS, Inc., Southpointe, 2017).